JOURNAL OF MATERIALS SCIENCE **36** (2001) 5357–5367

On the nano-size intergrowth of $Sr_4Fe_6O_{13\pm\delta}$ and $(Sr_{1-x}La_x)FeO_{3-\delta}$ phases in the mixed conductor $Sr_{3.6}La_{0.4}Fe_6O_z$

A. BARDAL
SINTEF Materials Technology, N-7465 Trondheim, Norway

R. BREDESEN
SINTEF Materials Technology, P.O. Box 124 Blindern, N-0314 Oslo, Norway
E-mail: rune.bredesen@matek.sintef.no

The microstructures of mixed-conducting $Sr_4Fe_6O_{13\pm\delta}$, and $Sr_{3.6}La_{0.4}Fe_6O_z$ (nominal composition) have been studied by electron microscopy. The lanthanum free material shows a microstructure containing mainly $Sr_4Fe_6O_{13\pm\delta}$, with some 5 vol% $Sr_{1-y}La_yFe_{12}O_{19}$ embedded as micron-size inclusions. The lanthanum-containing material revealed a significantly different microstructure consisting of ~20 vol% micron-size $Sr_{1-y}La_yFe_{12}O_{19}$ embedded in ~40 vol% $(Sr_{0.85}La_{0.15})FeO_{3-\delta}$ tetragonal perovskite, and ~40 vol% of plate-shaped nano-scale intergrowths between $(Sr_{1-x}La_x)FeO_{3-\delta}$ and $Sr_4Fe_6O_{13\pm\delta}$ phases. Domains with dimensions of 20–50 nm are observed in the tetragonal perovskite when viewed along its fourfold axis. From compositional analysis it is concluded that there is little or no solubility of La in the $Sr_4Fe_6O_{13\pm\delta}$ phase. The observed microstructure is important input in explaining the significant effect of La addition on the transport properties of $Sr_4Fe_6O_{13\pm\delta}$ materials.

1. Introduction

At present there is considerable focus on oxides that exhibit a mixed electronic and oxygen ion conductivity. These materials hold great promise for industrial use, e.g. as membranes providing oxygen for natural gas conversion or for pure oxygen production [1–3]. In operation the driving force for the flow of oxygen through the mixed conducting membranes is the oxygen partial pressure difference of the two sides of the membrane. The total flux of oxygen through the membrane depends on the simultaneous diffusion of oxygen ions and electrons, and the gas-membrane surface reactions involving dissolution and evolution of oxygen. The rate limiting process for the mass transport can be bulk transport or surface kinetics, and will depend on the membrane thickness, ambient gas composition and temperature.

A large number of different materials have been investigated as potential mixed conducting membranes [4]. These include two-phase composites, perovskites and perovskite related materials. In particular, the material $SrFeCo_{0.5}O_n$, for which an oxygen ion conductivity of 7 Scm^{-1} and electronic conductivity of 17 Scm^{-1} in air at 800°C have been reported [5], has been given much attention. Neutron and X-ray diffraction, SEM-EDS and EPMA-WDS studies have shown that this material consist of at least 3 phases, a perovskite phase ($SrFe_{1-x}Co_xO_{3-\delta}$), a layered perovskite related phase ($Sr_4Fe_{6-x}Co_xO_{13\pm\delta}$) and Fe-Co-oxide phases (usually spinel) [6, 7]. The layered perovskite related phase ($Sr_4Fe_{6-x}Co_xO_{13\pm\delta}$) was found to contain iron in the perovskite-like layer of corner shearing FeO_6 octahedra, and cobalt and iron in the separating double layer of five-coordinated $(Fe,Co)O_5$ and four-coordinated $(Fe,Co)O_4$ polyhedra [6].

The unusually large oxygen ion conductivity of the multi phase $SrFeCo_{0.5}O_n$ material, and the possibility of important interstitial oxygen diffusion in one of its major constituents ($Sr_4Fe_{6-x}Co_xO_{13\pm\delta}$) [8] lead to an investigation of the effect of higher valent cation dopant on the transport properties. As an attempt to increase the oxygen ion conductivity in the $Sr_4Fe_6O_{13\pm\delta}$, phase (assuming dominating interstitial oxygen diffusion), 10 mol% Sr was substituted with La. It was found that La substitution increased the conductivity and oxygen up-take in the membranes, and that these changes were probably a result of significant changes in phase composition by the formation of a large amount of perovskite phase [9]. Furthermore, it was found that the substitution resulted in a nano-sized intergrowth between the perovskite $(Sr_{1-x}La_x)FeO_{3-\delta}$ and the layered perovskite-like $Sr_4Fe_6O_{13\pm\delta}$ phases. In the present article, extended and more detailed microstructural and microanalytical characterization of $Sr_4Fe_6O_{13\pm\delta}$ (SFO) and membranes with nominal composition $Sr_{3.6}La_{0.4}Fe_6O_z$ (SLFO) is reported. It is also shown how the results of the microstructural analysis may throw light on the significant effects La addition has on the transport properties of $Sr_4Fe_6O_{13\pm\delta}$.

2. Experimental

Membranes were made by tape casting calcined powders of overall composition $Sr_4Fe_6O_{13\pm\delta}$ and $Sr_{3.6}La_{0.4}Fe_6O_{13\pm\delta}$. After drying, the green tapes were calcined at (1180 ± 5)°C for 5 hours, and were then cooled at a rate of 4°C/min to room temperature (RT). The membranes were then used in transient thermogravimetric measurements, where the atmosphere was changed between air and pure oxygen. These measurements were conducted by starting at 1100°C and then by step-wise reduction of 50°C repeating the measurements down to 700°C. Finally, the furnace was turned off, and the membranes were cooled to room temperature. A more detailed description of the materials synthesis is given in [8, 9]. The microstructural characterisation reported here was carried out on tape cast membranes before and after they were used in the thermogravimetric measurements.

The tape cast membranes were crushed down and investigated by powder XRD in a Siemens D5000 diffractometer using Cu K_α radiation. Diffractograms were simulated using public domain software [10] and structure data found in [11, 12]. Scanning electron microscopy (SEM) of mechanically polished sections of the membranes was carried out both in the cross-section and plan-view geometries, using a JEOL JSM 6400 equipped with a tungsten filament and operated at 10 kV. Microprobe analysis (EPMA) was done using a JEOL Superprobe JSM 8900 operated at 15 kV. Compositions were measured quantitatively using the ZAF procedure, based on experimental standards for the cations obtained from certified oxide standards.

Electron diffraction and microanalysis (EDS and EELS) was carried out using a Philips CM30 transmission electron microscope (TEM) operated at 200 kV, equipped with a Gatan PEELS system and an EDAX EDS system equipped with an ultrathin-window detector. A liquid-nitrogen cold stage was used for the microanalytical work. High-resolution electron microscopy (HREM) was done using a JEOL 4000 EX operated at 400 kV. Quantitative EDS was done by the commonly used Cliff-Lorimer method [13], and using k factors experimentally determined on our microscope. $k_{\mathrm{La,Fe}} = 2.55$ (referred to wt%) was determined using a $LaFeO_3$ standard and $k_{\mathrm{Sr,Fe}} = 1.96$ (referred to wt%) was determined using a $Sr_4Fe_6O_{13\pm\delta}$ standard.

Specimen preparation for TEM consisted in mechanical polishing and dimple grinding (avoiding water), followed by ion milling using a Gatan Duo Mill and a liquid-nitrogen cooled specimen holder. Specimen preparation for SEM was done by embedding in epoxy followed by careful mechanical polishing by hand (avoiding water), to minimize pull-out of phases. Despite the care taken, it was difficult to obtain a pore-free, perfect polish. Polished sections were coated with carbon before SEM examination.

3. Results

As mentioned the membranes were studied before and after thermogravimetric (TG) experiments. X-ray diffraction and electron microscopy revealed

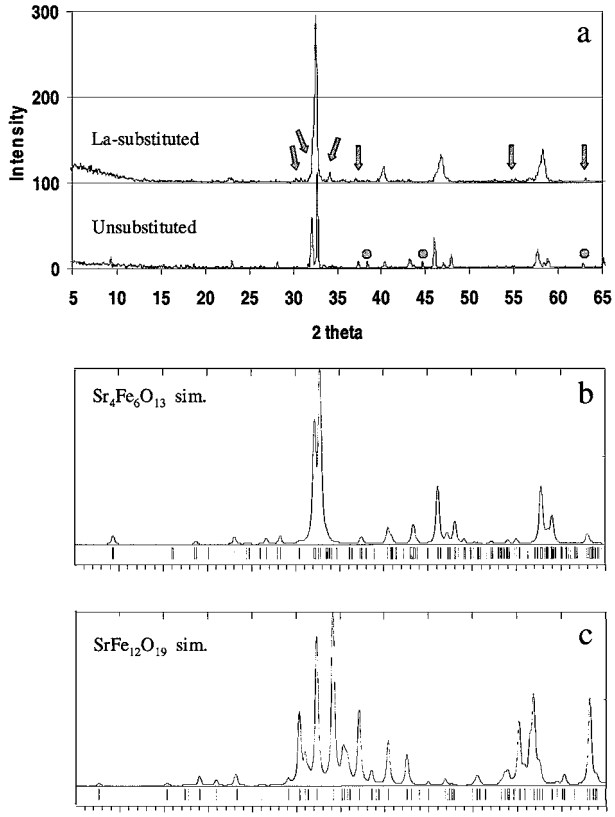

Figure 1 (a) X-ray diffractograms from La-containing and La-free materials. Arrows correspond to strongest $SrFe_{12}O_{19}$ lines and circles mark lines from sample holder. (b, c) simulated diffractograms for $Sr_4Fe_6O_{13}$ and $SrFe_{12}O_{19}$.

essentially no changes in the bulk microstructure or composition in the membranes after the TG. The surfaces of the membranes, however, were shown by SEM to undergo significant microstructural changes during the TG experiments [9]. Fig. 1 shows X-ray diffractograms from tape cast materials before TG experiments, and simulated diffractograms for $Sr_4Fe_6O_{13}$ (4-6-13) and $SrFe_{12}O_{19}$ (1-12-19). XRD from the La-free membranes shows that this material consists essentially of the 4-6-13 phase. Apart from three lines marked by circles in Fig. 1 (arising from the sample holder), all observed lines are consistent with 4-6-13. The peak at $2\theta = 9°$ corresponds to the 4-6-13 (010) planes with the largest spacing ($d = 19$ Å). Diffractograms from the La-containing membranes show new lines arising from a significant amount of 1-12-19. Contribution from 4-6-13 is again recognized, but now these lines form part of broader unresolved maxima. The major unresolved maxima are found at 2θ values of approximately 33°, 40°, 47°, and 58°. The results indicate a more complex microstructure and the presence of several structurally related phases.

SEM shows a homogeneous multiphase bulk microstructure independent of the position in the membrane, both for the SFO membrane and the SLFO membrane. The backscattered electron (BE) images shown in Fig. 2 reveal two distinctly different levels of grey for SFO, originating from two different phases. The dark phase can be identified as 1-12-19, and the grey phase as 4-6-13, on the basis of the XRD results and qualitative EDS measurements of phase composition in the SEM. Crude estimates of volume fractions

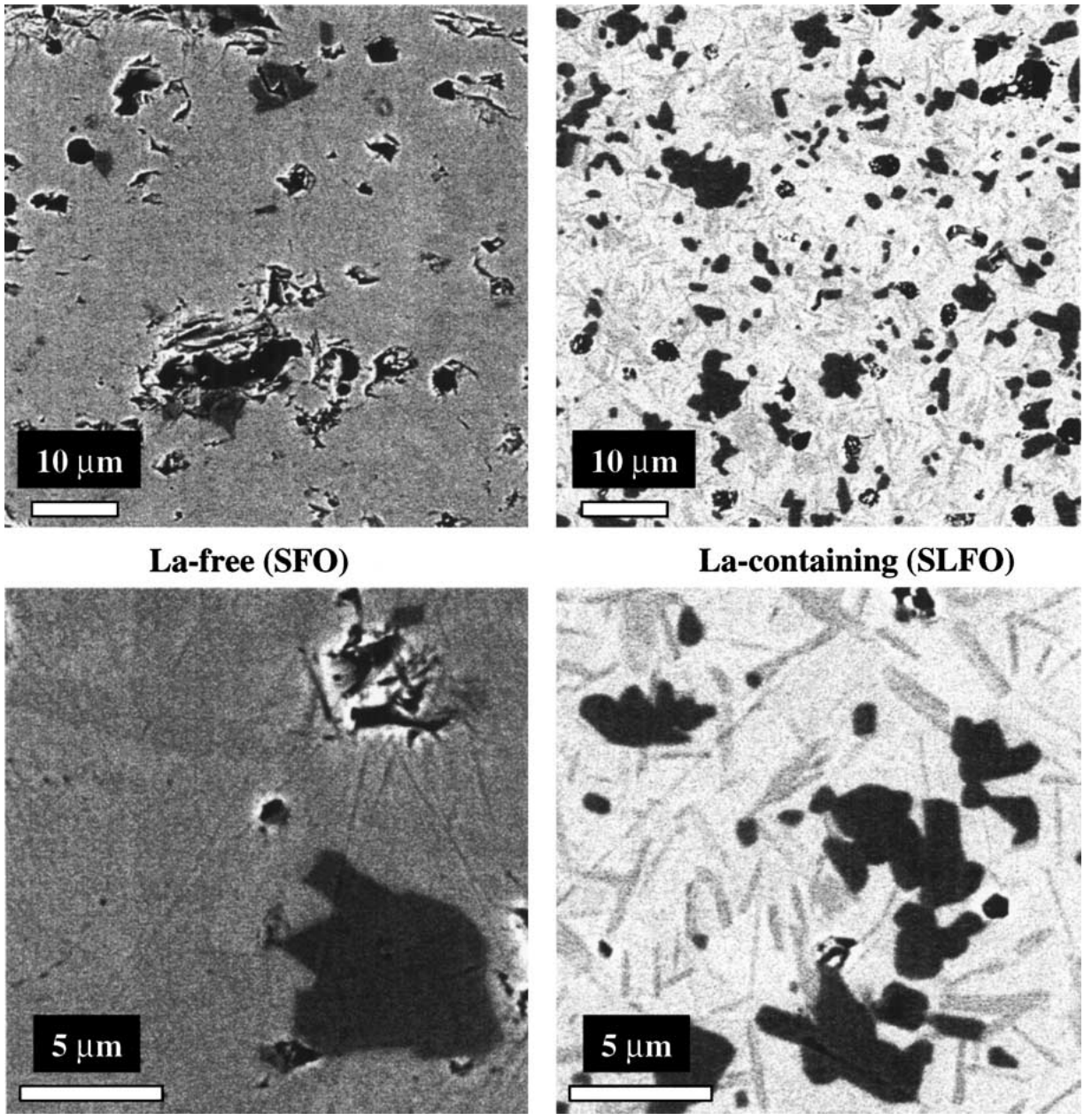

Figure 2 SEM images (backscattered electrons) from La-containing and La-free materials.

from the SEM images yield approximately 5 vol% of 1-12-19 for the SFO sample. Very weak grey-level variations can furthermore be observed in the 4-6-13 matrix in SFO (Fig. 2). It is not likely that these variations are due to different phases, as discussed later. The variations may be channeling contrast, arising from different crystallographic orientation of the different 4-6-13 grains. The BE images from the SLFO sample reveal three distinctly different levels of grey, originating from three different compositions. On the basis of TEM studies, to be reported in more detail below, these BE images can be interpreted as follows:

The bright regions are a perovskite phase, $(Sr_{1-x}La_x)FeO_{3-\delta}$. For simplicity we will call this phase 1-1-3. The grey regions are fine-scale intergrowths between 1-1-3 and a phase with a long axis ($b \approx 19$ Å), most probably the 4-6-13 phase. The dark regions are the 1-12-19 phase.

Crude estimates of volume fractions from the SEM images yield approximately 20 vol% of 1-12-19, 40 vol% of 1-1-3, and 40 vol% of intergrowth regions (1-1-3 plus 4-6-13) for the SLFO sample. Precise measurements of volume fractions cannot easily be made given the difficulties with SEM sample preparation, resulting in a significant amount of preparation-induced voids in the surface.

Fig. 3 shows a $SrFe_{12}O_{19}$ particle in SLFO, as identified by selected-area diffraction (SAD) and EDS. These particles have a rounded shape and typical size 1–5 μm. Fig. 4 shows a low-magnification TEM image from SLFO. Characteristic plate-shaped grains have a high density of planar faults. Other grains have more rounded shapes and no striking defect densities. The arrowed grain exhibits streaky contrast from defects to the left and smooth, defect-free contrast to the right. The corresponding SAD patterns and EDS spectra show that two different phases are present. SAD tilt series and single SAD patterns along low-index zone axes from several particles with smooth contrast indicated that the predominant phase is a body-centred tetragonal phase

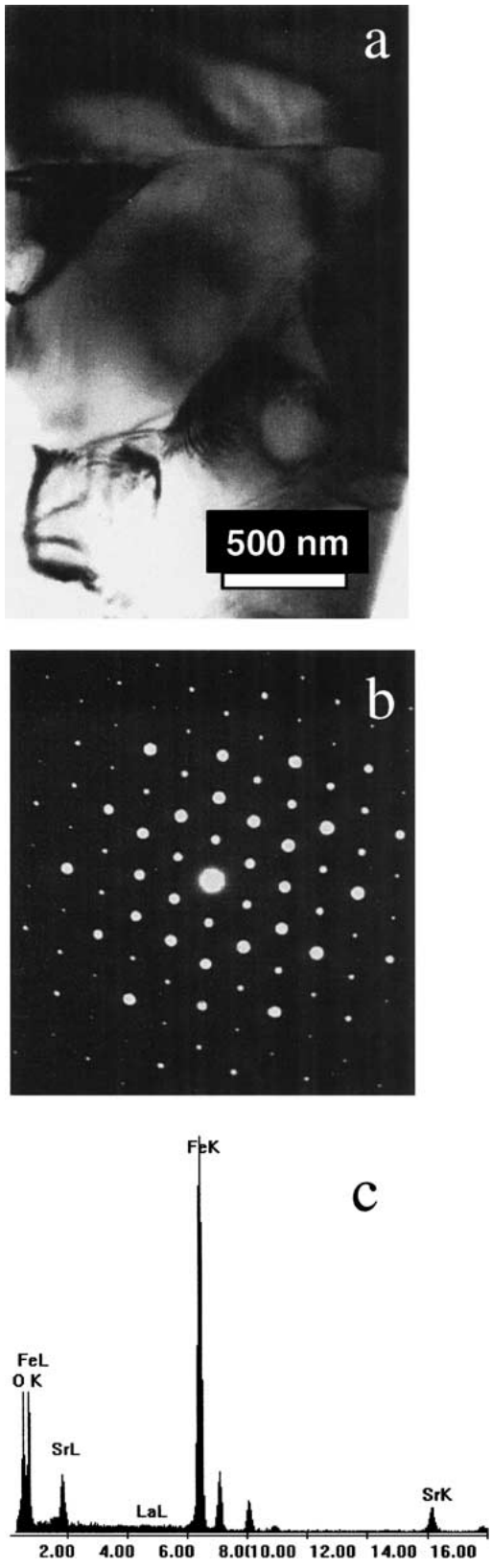

Figure 3 (a) Bright-field TEM image, (b) selected-area diffraction pattern along the six-fold [0001] zone axis, and (c) EDS spectrum from $Sr_{1-z}La_zFe_{12}O_{19}$.

with $a \approx c \approx 11.0$ Å and $b \approx 7.9$ Å. On one occasion, SAD patterns were also recorded that could not be indexed as body-centred tetragonal. These were consistent with base-centred orthorhombic, $a \approx 11.0$ Å, $b \approx 7.7$ Å, $c \approx 5.5$ Å. These different perovskite phases yield quite similar electron diffraction patterns, but can be distinguished on the basis of their extinctions and shortest g-vectors, particularly when viewed along the lowest-index zone axes.

Fig. 5 shows HREM images from the streaky part of the grain arrowed in Fig. 4. HREM reveals that the streaky contrast originates from an irregular intergrowth of two different phases on $a \sim 10$ nm lengthscale. By analyzing tilt series (bearing in mind that SAD patterns from the highly defective grains are a superposition of patterns from two different phases) and measuring interplanar distances in the HREM images, the intergrowth phases can be identified. One phase is the tetragonal perovskite 1-1-3 phase discussed above. The other phase has $a \approx 5.5$ Å or ≈ 11.0 Å, $c \approx 5.5$ Å or ≈ 11.0 Å, and $b \approx 19.0$ Å. There is still uncertainty in the determination of the short axes because of contribution in the SAD patterns from the perovskite phase. The phase is likely to be $(Sr_{1-y}La_y)_4Fe_6O_{13\pm\delta}$, since the SAD results may well be consistent with the reported structure for 4-6-13, i.e. orthorhombic, space group *Iba*2, $a = 11.10$ Å, $b = 18.92$ Å, $c = 5.57$ Å [11].

The relative amounts of 1-1-3 and 4-6-13 in the intergrowth regions vary significantly from place to place. Whereas the phases were present in nearly equal amounts in the example shown in Figs 4 and 5, Fig. 6 shows a different situation. Here the structure is predominantly 4-6-13, with only thin (1–2 unit cells) isolated lamellae of 1-1-3. The intergrowth is most easily revealed when viewed perpendicular to the stacking direction, i.e. perpendicular to: $[010]_{4\text{-}6\text{-}13}||[010]_{1\text{-}1\text{-}3}$.

When viewed along the fourfold [010] axis of the tetragonal 1-1-3 phase, a fine domain structure is revealed. Low-magnification bright-field images were found to exhibit characteristic tweed-like contrast indicative of nano-domains. HREM revealed rectangular domains of typical linear dimensions 20–50 nm, Fig. 7, and thinner lamellae of width 2–3 nm. The SAD pattern in Fig. 7c has contribution from a large number of nano-domains. All major reflections are consistent with the tetragonal 1-1-3 phase. Fast-Fourier-transform (FFT) diffractograms obtained from different regions of dimensions 7×7 nm^2 within individual domains showed that these were essentially identical and revealed the same spatial frequencies as the depicted SAD pattern. The thin lamellae could not easily be analyzed by FFT, owing to their small size. The high-magnification HREM image of Fig. 7b exhibits no striking contrast variations inside the domains, apart from those assumed to have arisen from specimen tilt and thickness.

Fig. 8 shows a low-magnification TEM micrograph from the La-free material. The grains have characteristic plate shape, and are found to exhibit a streaky contrast indicative of a high density of planar defects. No TEM observations of perovskite grains with smooth defect-free contrast were made in SFO. Also, apart from the small amounts of 1-12-19 observed in this material, XRD gives no indications of other secondary phases. EDS measurements of the Sr:Fe ratios in the SEM yielded no significant variations except when measuring in 1-12-19. All these observations are consistent with the material being 4-6-13 with a small amount of 1-12-19 inclusions. It is therefore likely that the weak

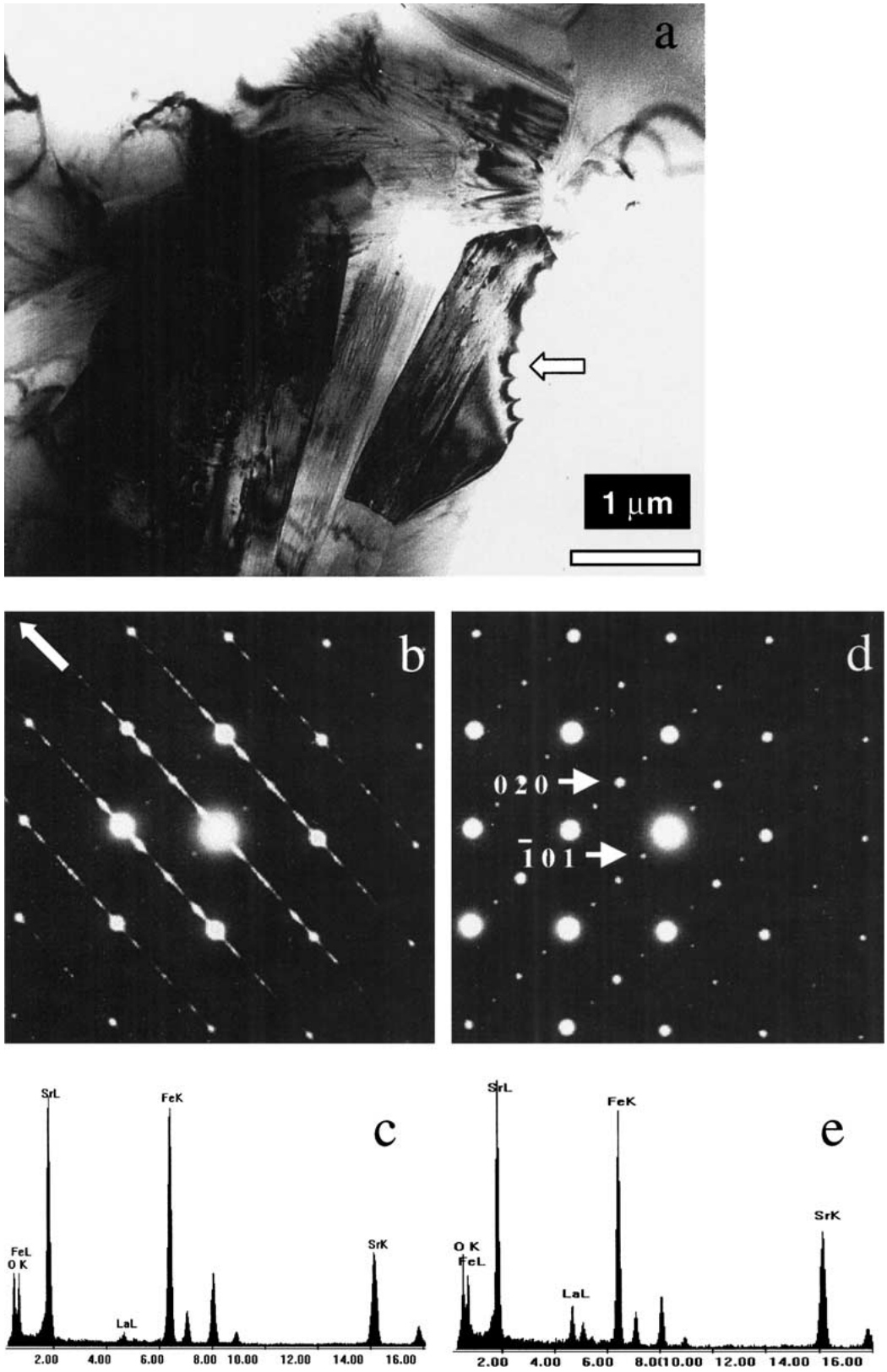

Figure 4 (a) Bright-field TEM image of the typical microstructure of the La-containing material. (b) Selected-area diffraction pattern from faulted part of arrowed grain. The densely spaced reflections along the arrowed direction correspond to a lattice parameter of 1.9 nm. (c) EDS spectrum from faulted part of arrowed grain exhibiting low La content. (d) Selected-area diffraction pattern from unfaulted part of arrowed grain, indexed as tetragonal perovskite viewed along the [1 0 1] zone axis. The TEM specimen orientation is the same as for (b). (e) EDS spectrum from unfaulted part of arrowed grain exhibiting higher La content.

contrast variations seen in the matrix of SFO (Fig. 2) has a different explanation, such as channeling contrast. However, it is reasonable to assume that small domains or planar defects related to local variations in composition and structure may exist in the 4-6-13 matrix due to the presence of the 1-12-19 phase. Detailed electron diffraction or HREM analysis of this material has not yet been undertaken, so the detailed origin of the streaky contrast and the nature of planar defects are still not clear.

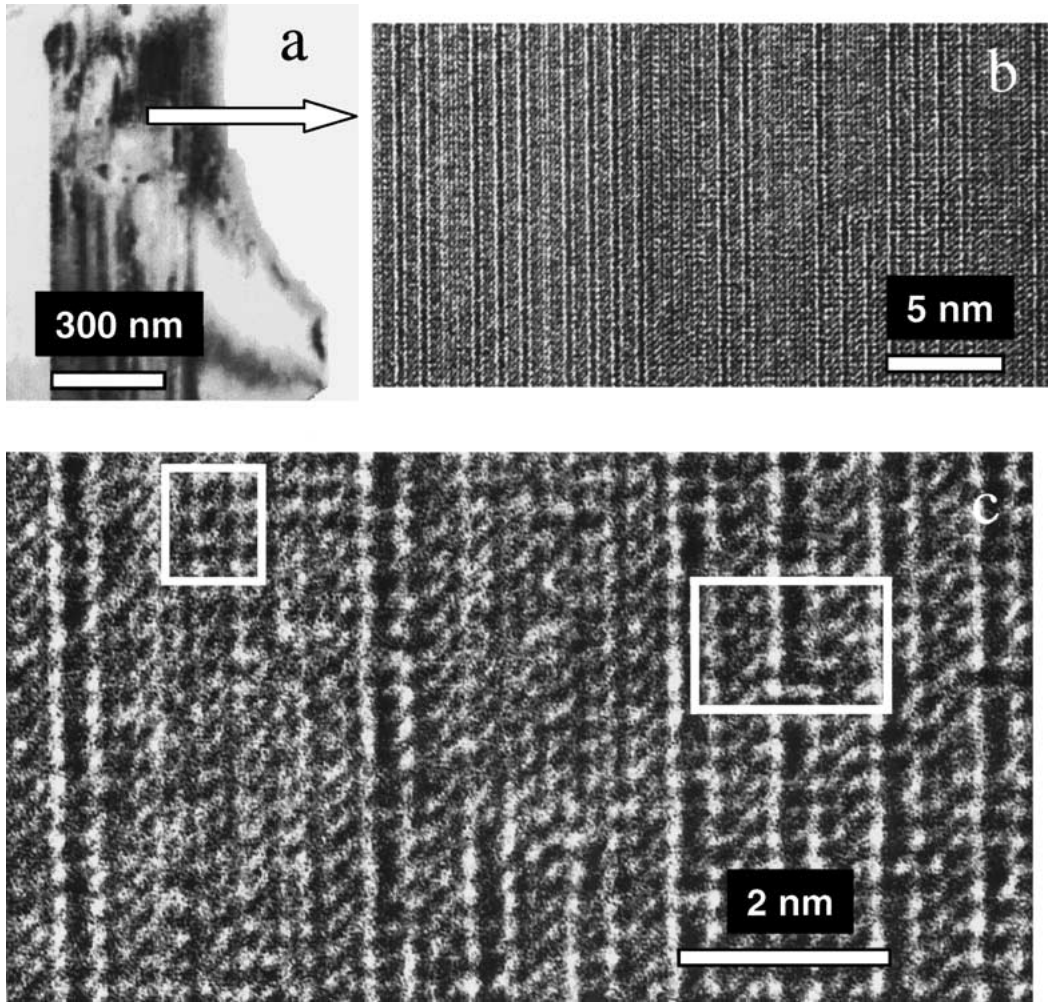

Figure 5 (a) Bright-field TEM image of selected grain. (b, c) High resolution electron micrographs (HREM) from faulted part of the grain, at increasing magnification. The frames indicate unit cells of $Sr_{1-x}La_xFeO_{3-\delta}$ (left) and $Sr_4Fe_6O_{13\pm\delta}$ (right) viewed along their [001] directions.

The compositions of the different phase-regions were measured using WDS in the EPMA (SLFO sample), and using EDS in the TEM (SLFO and SFO samples). EDS measurements from SFO were in all cases within 5% of Fe:Sr = 1.5, in accordance with the overall nominal composition, and with the stoichiometry of the 4-6-13 phase. Results from SLFO are summarized in Fig. 9. Here both results from EDS in TEM and WDS in EPMA are included in the same plot. The main difference between these measurements is that the WDS probed an interaction volume on the order of 1 μm large, whereas the diameter of the electron beam used for the EDS recordings was approximately 30 nm. Compositional results obtained with the two techniques are in good accordance with each other. EPMA showed no significant differences in the composition of bulk phases in the materials before and after the TG experiments.

4. Discussion

4.1. Microstructural and phase compositional considerations

The compositional measurements showed that the La:Sr ratio is significantly higher in the perovskite 1-1-3 phase than in the nano-scale intergrowth regions. All measurements of the perovskite gave La:(La + Sr) ratios of 0.15 ± 0.01. Significant variations in the La:(La + Sr) ratio were found in the intergrowth regions. Results from these regions represent an averaged composition depending on the proportions of 4-6-13 and 1-1-3 phases in the probed volumes. The La:(La + Sr) variations are therefore likely to be due to varying proportions between the 1-1-3 and 4-6-13 phases. The data follow an approximately straight line between the compositions 4Sr-6Fe and 0.85Sr-0.15La-Fe, indicating that the La content in the 4-6-13 component of the intergrowth is very close to zero. There are no significant differences between EDS and WDS data from the intergrowth regions. This implies that phase proportions mainly vary between the different regions (medium gray in Fig. 2), rather than inside the individual regions. The average La:(La + Sr) ratio in the intergrowth regions was determined as 0.05.

The results clearly demonstrate that the 4-6-13 phase cannot accommodate much lanthanum. Instead of being incorporated in the 4-6-13 structure (as was the intention for increasing the amount of interstitial oxygen), the presence of La leads to the formation of large amounts of perovskite, along with 1-12-19. The reported 4-6-13 structure [11] can be described as a stacking of perovskite ($SrFeO_3$) and $Fe_2O_{3-\delta}$ layers, where the iron atoms of the perovskite layers are octahedrally coordinated. Due to the similarity between the 1-1-3 and 4-6-13 structures it is not obvious why the 4-6-13 structure does not accommodate a noticeable amount of

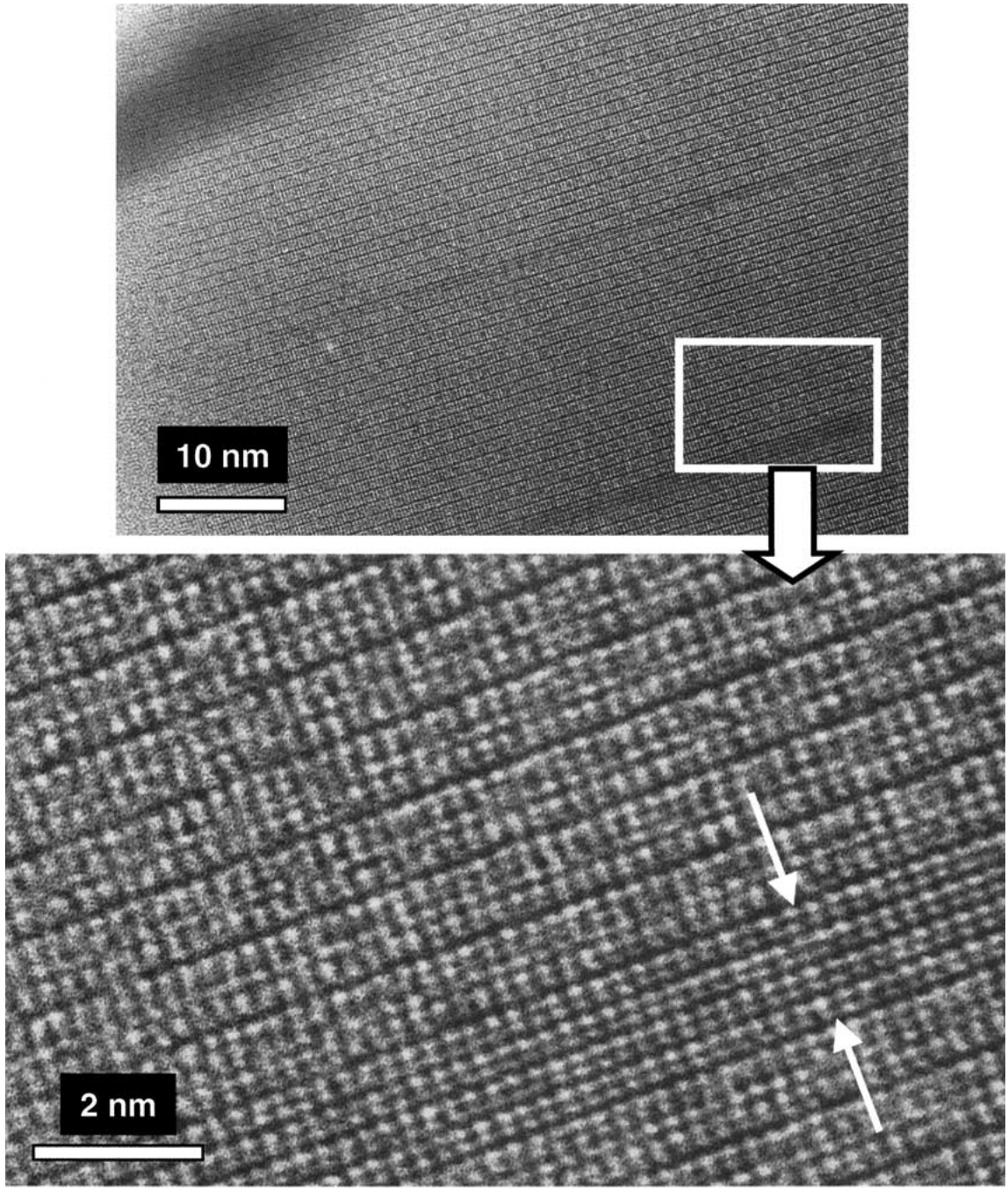

Figure 6 HREM of intergrowth region with high proportion of $(Sr_{1-y}La_y)_4Fe_6O_{13\pm\delta}$ phase. Only thin lamellae (1–2 unit cells) of perovskite are found, as marked by arrows.

lanthanum. Substitution of La for Sr in the perovskite layers, along with filling of oxygen in $Fe_2O_{3-\delta}$ layers can be envisaged in the 4-6-13 structure. No reports of such substitution can be found in the literature, however, and there is no 4-6-13 phase in the reported La_2O_3-Fe_2O_3 phase diagram [14]. Accordingly, our results demonstrate clearly that it is more favorable to form the La-containing perovskite than substitute for Sr in 4-6-13.

The results show some solubility of La in 1-12-19, as La:Sr ratios of 0.05 were regularly measured, both by EDS in the TEM and by EPMA. Noting that $LaFe_{12}O_{19}$ is isostructural with $SrFe_{12}O_{19}$ [12,14], this is not surprising. We are not of aware of reported studies of La:Sr solubility in 1-12-19, nor have we carried out detailed studies of this.

The ability of $SrFeO_{3-\delta}$ to accommodate La on Sr sites is well known, but literature is incomplete in describing the different structural modifications in this system. $SrFeO_{3-\delta}$ tolerates a large oxygen deficit and takes different structures as δ varies from zero to 0.5. The fully oxidized phase ($\delta = 0$) has the simple cubic perovskite structure with $a = 3.86$ Å at RT. The structure of $SrFeO_{2.5}$ (brownmillerite) is orthorhombic, space group *Ibm*2, $a = 5.66$ Å ($\approx\sqrt{2}\,a_C$), $b = 15.60$ Å ($\approx 4\ a_C$), $c = 5.53$ Å ($\approx\sqrt{2}\,a_C$) [15]. Takeda and coworkers [16] furthermore found two phases for intermediate oxygen stoichiometries and gave the following structural data (without giving complete structural descriptions). For $3-\delta \approx 2.86$: Body-centred tetragonal with $a = 10.93$ Å ($\approx 2\sqrt{2}\,a_C$), $c = 7.71$ Å ($\approx 2\,a_C$). For $3-\delta \approx 2.75$: Base-centred orthorhombic

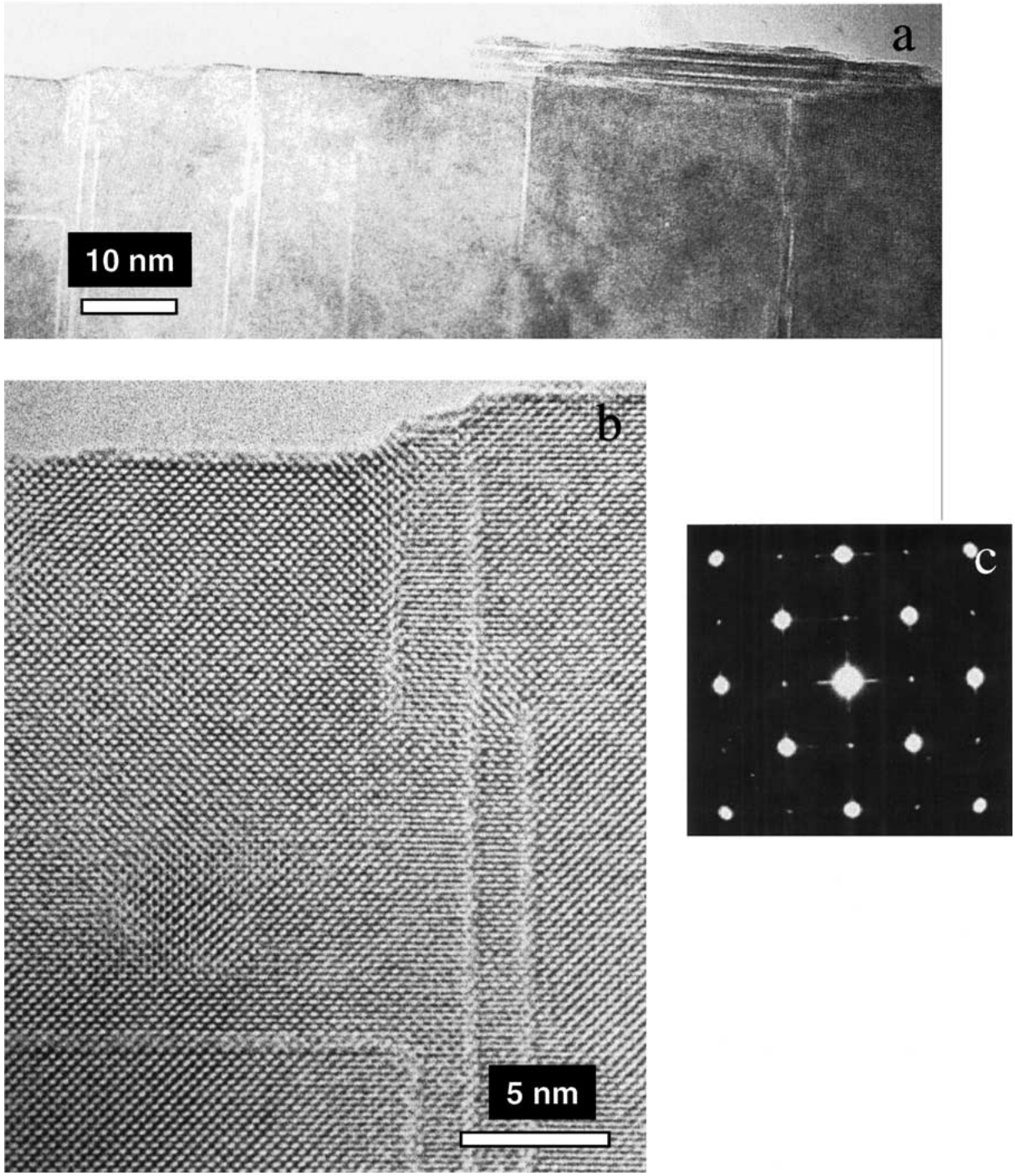

Figure 7 (a, b) HREM of domain structure in $Sr_{1-x}La_xFeO_{3-\delta}$ as viewed along the fourfold [010] zone axis. (c) Corresponding selected-area diffraction pattern.

with $a = 10.97$ Å ($\approx 2\sqrt{2}\,a_C$), $b = 7.70$ Å ($\approx 2\,a_C$), $c = 5.47$ Å ($\approx \sqrt{2}\,a_C$). Intermediate compositions were found to exhibit mixtures of these phases [16]. Several groups have observed that samples cooled slowly in air exhibit an oxygen content of $3 - \delta = 2.80$–2.85 [16–19]. Dann and coworkers [20] published an extensive study of the phases present in $Sr_{1-x}La_x$ $FeO_{3-\delta}$ after slow cooling to room temperature, with x varying from zero to one. For low La contents (<0.2) like in our material, they report mixtures between cubic and tetragonal phases, without giving complete structural descriptions. Battle and coworkers [21–23] studied structure variations and vacancy ordering as a function of oxygen content in $(Sr_2La)FeO_{3-\delta}$. They found strong similarity with the Sr-Fe-O system, i.e. evidence for ordered-vacancy phases, and transition from (weakly) rhombohedral to tetragonal to orthorhombic structures with increasing δ. In none of the above mentioned investigations have intergrowth of the two phases 1-1-3 and 4-6-13 been observed. All defect ordering and structural modifications reported have dealt with variations of the perovskite structure.

Our identification of a body-centered tetragonal perovskite with a La:(La + Sr) ratio of 0.15 is in good agreement with the above mentioned reports. The structure we have found is fully consistent with the tetragonal perovskite phase reported by Takeda and coworkers [16]. There is good reason to believe that

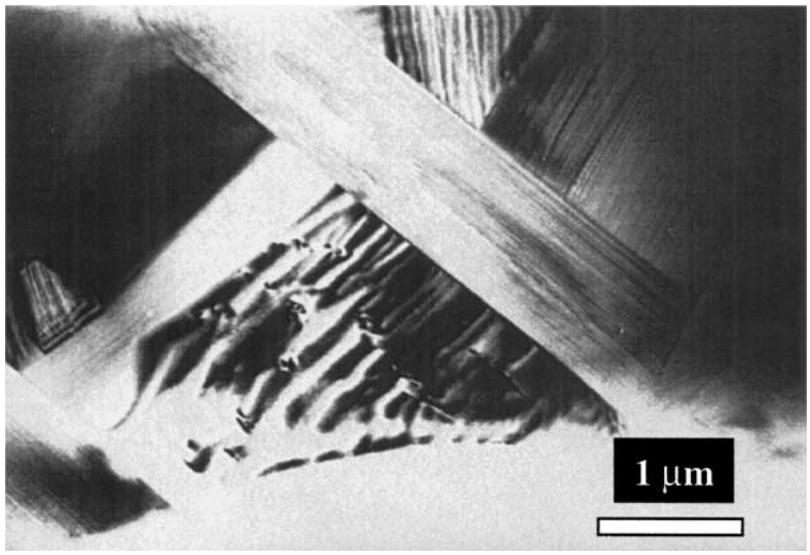

Figure 8 Bright-field TEM image of the typical microstructure of the La-free material.

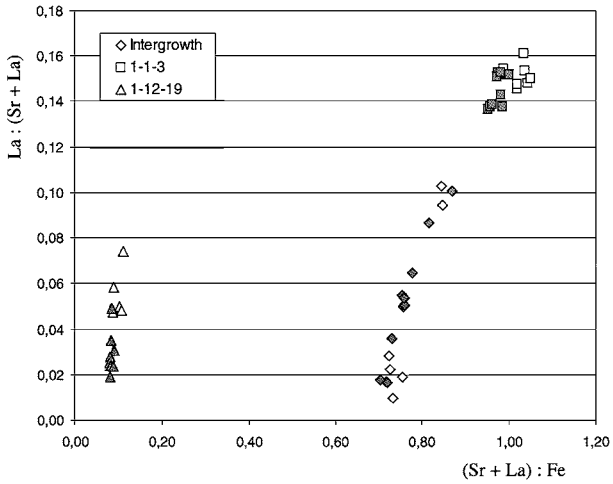

Figure 9 Composition of the three phases in the La containing material, as measured by WDS/EPMA (filled symbols) and EDS/TEM (open symbols).

$3-\delta \approx 2.875$ is the oxygen content of the tetragonal phase in our case, since the structure represents a certain ordering of oxygen vacancies, as discussed in [24]. We made preliminary measurements of oxygen content in 1-1-3 using EELS, which yield an Fe:O ratio in between 1:3 and 1:2.5. The precision of these measurements was, however, yet to poor for firm conclusions to be drawn. With SAD we made one observation consistent with the orthorhombic perovskite with $3-\delta \approx 2.75$, reported in [16], which indicates that the overall oxygen content in our perovskite phases is on the low side of $3-\delta = 2.875$.

The observation of nanodomains when viewed along the tetragonal perovskite [001] direction is a further indication of deviations in the overall perovskite oxygen content from $3-\delta = 2.875$. The presence of tetragonal perovskite alone would not yield the observed kind of domain formation. With a truly tetragonal structure the domains seen in Fig. 7b are crystallographically identical. Hence, the concept of orientation variants does not apply in the depicted situation. The key to understanding the observed domain structure may lie in the domain walls, and possible deviations in local composition in these. Domain formation has been reported for the related $Ca_{1-x}La_xFeO_{3-\delta}$ system. In the fully reduced $Ca_2LaFe_3O_8$ orientation variants of a single brownmillerite phase were found to form small domains [25]. In partly reduced $Ca_xLa_{1-x}FeO_{3-\delta}$ a mixture of two phases was observed to be present as small domains [26]. In the latter case, it was suggested that the domain walls contained excess oxygen.

The x-ray diffractogram from the La-containing membrane (Fig. 1.) can be understood from the electron microscopy results. The broadened maxima have contributions from 4-6-13 as well as split (compared to cubic perovskite) lines from the tetragonally distorted perovskite. The individual lines are furthermore broadened because of the small size of the lamellae in the intergrowth regions. In the La-containing membranes, perovskite is found both as separate grains and within intergrowth regions. Membranes not used in the TG measurements also showed the nanosized intergrowth, and the possibility that such intergrowth structure may exist at the calcination temperature of 1180°C, is real. One may assume that the excess energy of the intergrowth is small and provides only a weak driving force for any rearrangements of cations. This may therefore explain the small size, however, slow formation during cooling may also give rise to such small size.

The TEM studies reported here were done on samples that had been slowly cooled in air from temperatures of 700°C (TG samples) or higher. Hence, the results yield no information on oxygen content at the temperatures and oxygen partial pressures of the TG or conductivity measurements (700°C–1100°C). In this context it is worth noting that high-temperature XRD [19] shows that the vacancy ordering schemes reported by Takeda and coworkers [16] only appear below approximately 400°C.

4.2. Transport properties and defect chemistry considerations

The transport properties and defect chemistry of 1-1-3 and 4-6-13 are still a matter of discussion [27–30]. The following experimental observations should be noticed:

1. When the temperature is reduced from around 1150°C to 1000–800°C, the conductivity of $Sr_{3.6}La_{0.4}Fe_6O_z$ does not reach a stable value but slowly decreases for days [9]. If the material is again heated at high oxygen pressure at 1150°C, the initial high conductivity is restored.

2. The conductivity of 4-6-13 is lower than 1-1-3 at high oxygen pressures, and higher than 1-1-3 at low oxygen pressures [9, 30].

3. When the oxygen partial pressure is changed from air to 1 atm. oxygen, the oxygen up-take is higher in $Sr_{3.6}La_{0.4}Fe_6O_z$ than in La-free 4-6-13 [8].

Compared to the perovskite, the 4-6-13 phase is thermodynamically stabilised at moderate temperatures and moderate to high oxygen partial pressures. At high temperatures and reduced oxygen partial pressures, a phase transition to the perovskite may occur [28]. The observations in point 1 above may now be understood in light of the microstructural findings. At high oxygen partial pressure and temperature, the material has a high content of 1-1-3. As the temperature is lowered a slow transition of 1-1-3 to 4-6-13 occurs, probably by consuming the 1-12-19 phase according to

$$(42/11)SrFeO_{3-\delta 1} + (2/11)SrFe_{12}O_{19} \Rightarrow Sr_4Fe_6O_{13\pm\delta 2} \quad (1)$$

(for simplicity neglecting La).

Since the p-type electronic conductivity is higher in 1-1-3 than 4-6-13 at high oxygen partial pressures (point 2), a reduction in conductivity can be expected when reducing the temperature. Moreover, when changing the partial pressure of oxygen from high to low values at constant temperature in the region 800–1000°C, the perovskite is expected to be formed by the reverse reaction 1. At reduced oxygen partial pressure the perovskite can be expected to have ordered oxygen vacancies, i.e. the structure is the brownmillerite type. Under these conditions the 1-1-3 material has lower conductivity than the 4-16-13 material, and again a reduction in conductivity can be expected (point 1). The very slow changes observed in the conductivity suggest that the phase transitions are extremely slow. The observed nano-size intergrowth of the 1-1-3 and 4-6-13 therefore probably stems from a low energetic driving force for the transition combined with the structural similarity. The fact that the high conductivity can be restored by high temperature annealing suggests that the formation of the nano-sized intergrowth is "reversible" in character. Finally, the higher oxygen take-up in the La-containing material compared to La-free 4-16-13 suggests that the concentration of oxygen defects is higher in the 1-1-3 phase than in the 4-6-13 phase. This is in accordance with the observation that the oxygen diffusion is higher in 1-1-3 than in 4-6-13 (e.g. seen by comparing values of the chemical diffusion coefficient in refs [28, 29]). This is also supported by a recently reported study on oxygen permeation rates in $SrFe_{1.5-m}Co_mO_n$ which shows that the perovskite phase has higher oxygen permeation than the 4-6-13 phase [27]. Thus, possible coexistence of these phases on a nano-sized level, as shown in the present study, should in future (as well in former) studies be considered.

In contrast to the La-containing material, the conductivity of the La-free 4-6-13 material appeared much more stable with time, which is expected from the considerations made above.

5. Conclusion

The mixed conductor $Sr_{3.6}La_{0.4}Fe_6O_z$ (nominal composition) has been found to consist of three phases. These are micron-size $Sr_{1-y}La_yFe_{12}O_{19}$ inclusions, $(Sr_{0.85}La_{0.15})FeO_{3-\delta}$ tetragonal perovskite, and a plate-shaped nano-scale intergrowth between $(Sr_{1-x}La_x)FeO_{3-\delta}$ and $Sr_4Fe_6O_{13\pm\delta}$ phases. The observations show that there is little or no solubility of La in $Sr_4Fe_6O_{13\pm\delta}$ and that the attempt to substitute Sr with La in $Sr_4Fe_6O_{13\pm\delta}$ yields the formation of large amounts of perovskite. Rectangular nanodomains of typical dimensions 20–50 nm are observed for the tetragonal perovskite when viewed along its fourfold axis. The observation of a phase mixture of the perovskite related $Sr_4Fe_6O_{13\pm\delta}$ and perovskite provides important input for explaining measured transport properties and their time dependencies in these materials.

Acknowledgements

We are grateful to M. P. Raanes and T. L. Rolfsen for the EPMA and XRD recordings, to T. Grande for helpful discussions, and to H. Cerva at Siemens Research Laboratories, Munich, for permission to use the JEOL 4000 EX.

References

1. B. C. H. STEELE, *Current Opinion in Solid State & Materials Science* **1** (1996) 684.
2. J. KILNER, S. BENSON, J. LANE and D. WALLER, *Chemistry & Industry* (1997) 907.
3. R. BREDESEN and J. SOGGE, Presented at the United Nation Seminar on the Ecological Applications of Innovative Membrane Technology in the Chemical Industry. Ref. UN Economic Commission for Europe, CHEM/SEM. 21/R.12, 13 March 1996, May 1–4, 1996, Cetraro, Italy.
4. H. J. M. BOUWMEESTER and A. J. BURGGRAAF, in "Fundamentals of Inorganic Membrane Science and Technology," edited by A. J. Burggraaf and L. Cot (Elsevier, Amsterdam, 1996) p. 435.
5. B. MA, U. BALACHANDRAN, J.-H. PARK and C. U. SEGRE, *J. Electrochem. Soc.* **143** (1996) 1736.
6. H. FJELLVÅG, B. C. HAUBACK and R. BREDESEN, *J. Mater. Chem.* **7** (1997) 2415.
7. R. BREDESEN, H. RÆDER, C. SIMON and A. HOLT, in Proceedings of the 5th International Conference on Inorganic Membanes, Nagoya, Japan, June 22–26 1998, p. 412.
8. R. BREDESEN, F. MERTINS and T. NORBY, *Catal. Today* **56** (2000) 315.
9. R. BREDESEN, T. NORBY, A. BARDAL and V. LYNUM, *Solid State Ionics*, in press.
10. G. NOLZE and W. KRAUS, PowderCell software, 1998. http://www.bam.de/a_v/v_1/powder/e_cell.html
11. A. YOSHIASA, K. UENO, F. KANAMARU and H. HORIUCHI, *Mater. Res. Bull.* **21** (1986) 175.
12. X. OBRADORS, X. SOLANS, A. COLLOMB, D. SAMARAS, J. RODRIGUEZ, M. PERNET and M. FONT-ALTABA, *J. Solid State Chem.* **72** (1988) 218.

13. D. B. WILLIAMS and C. B. CARTER, "Transmission Electron Microscopy" (Plenum Press, New York, 1996) p. 597.
14. V. L. MORUZZI and M. W. SHAFER, *J. Amer. Ceram. Soc.* **43** (1960) 367.
15. M. HARDER and HK. MÜLLER-BUSCHBAUM, *Z. Anorg. Allg. Chemie* **464** (1980) 169.
16. Y. TAKEDA, K. KANNO, T. TAKADA, O. YAMAMOTO, M. TAKANO, N. NAKAYAMA and Y. BANDO, *J. Solid State Chem.* **63** (1986) 237.
17. J. B. MACCHESNEY, R. C. SHERWOOD and J. F. POTTER, *J. Chem. Phys.* **43** (1965) 1907.
18. T. C. GIBB, *J. Chem. Soc. Dalton Trans.* (1985) 1455.
19. J. MIZUSAKI, M. OKAYASU, S. YAMAUCHI and K. FUEKI, *J. Solid State Chem.* **99** (1992) 166.
20. S. E. DANN, D. B. CURRIE, M. T. WELLER, M. F. THOMAS and A. D. AL-RAWWAS, *ibid.* **109** (1994) 134.
21. P. D. BATTLE, T. C. GIBB and S. NIXON, *ibid.* **79** (1989) 75.
22. P. D. BATTLE, T. C. GIBB and P. LIGHTFOOT, *ibid.* **84** (1990) 237.
23. *Idem.*, *ibid.* **84** (1990) 271.
24. M. TAKANO, T. OKITA, N. NAKAYAMA, Y. BANDO, Y. TAKEDA, O. YAMAMOTO and J. B. GOODENOUGH, *ibid.* **73** (1988) 140.
25. M. A. ALARIO-FRANCO, M. J. R. HENCHE, M. VALLET, J. M. GONZALEZ-CALBET, J. C. GRENIER, A. WATTIAUX and P. HAGENMULLER, *ibid.* **46** (1983) 23.
26. M. A. ALARIO-FRANCO, J. M. GONZALEZ-CALBET, M. VALLET-REGI and J. C. GRENIER, *ibid.* **49** (1983) 219.
27. T. ARMSTRONG, F. PRADO, Y. XIA and A. MANTHIRAM, *J. Electrochem. Soc.* **147** (2000) 435.
28. R. BREDESEN and T. NORBY, *Solid State Ionics* **129** (2000) 285.
29. A. HOLT, T. NORBY and R. GLENNE, *Ionics* **5** (1999) 434.
30. A. HOLT and T. NORBY, to be published.

Received 2 November 2000
and accepted 16 July 2001